Arabian Journal of Chemistry (2022) **15**, 104215

King Saud University

**Arabian Journal of Chemistry**

www.ksu.edu.sa
www.sciencedirect.com

ORIGINAL ARTICLE

# Chemical characterization and antioxidant, anti-inflammatory, and anti-septic activities of the essential oil from the aerial parts of *Atractylodes macrocephala* Koidz

**Lin-yan Wang [b,1], Mei-ya Li [b,1], Le-hao Jin [a,1], Yong-hua Wei [a], Jia-mao Wang [a], Jie-li Pan [b], Chun-chun Zhang [c], Chang-yu Li [b,*], Fu-sheng Jiang [a,*]**

[a] *College of Life Science, Zhejiang Chinese Medical University, Hangzhou 310053, PR China*
[b] *Academy of Chinese Medical Sciences, Zhejiang Chinese Medical University, Hangzhou 310053, PR China*
[c] *College of Pharmaceutical Science, Zhejiang Chinese Medical University, Hangzhou 310053, PR China*

Received 23 May 2022; accepted 17 August 2022
Available online 22 August 2022

**KEYWORDS**

Essential oil;
*Atractylodes macrocephala* Koidz.;
Chemical composition;
Antioxidant;
Anti-inflammatory;
LPS-induced septic shock

**Abstract** *Atractylodes macrocephala* Koidz. (AM) is a rhizome plant traditionally used as an herbal medicine to normalize gastrointestinal function and treat inflammation-related diseases. However, there are no comprehensive studies that have examined the chemical composition or biological activity of the aerial parts of AM, which may be a promising raw material for the pharmaceutical industry. The aim of this study was to investigate the constituents, anti-oxidant, anti-inflammatory and anti-septic activities of the essential oil of the aerial parts of *Atractylodes macrocephala* (EOAPA). The chemical composition analysis of EOAPA by gas chromatography-quadrupole-time of flight-mass spectrometry (GC-Q/TOF-MS) led to the identification of 73 components, and the dominant compounds were hinesol (12.61%), *β*-eudesmol (11.51%), and atractylone (5.8%). EOAPA significantly inhibited lipopolysaccharide (LPS)-induced RAW264.7 cell expression of monocyte chemokine-1 (MCP-1), interleukin-6 (IL-6), cyclooxygenase-2 (COX-2) and inducible nitric oxide synthase (iNOS) in a dose-dependent manner via regulating the nuclear transcription factor-κB (NF-κB) pathway, which may be related to its strong reactive oxygen species (ROS)-scavenging ability against LPS challenge at cellular level. While, its antioxidant activity in vitro was weak. Finally, LPS-induced septic shock in

* Corresponding authors.
E-mail addresses: lm159@sina.com (C.-y. Li), jfs1020@163.com (F.-s. Jiang).
[1] These authors have contributed equally to this work.

Peer review under responsibility of King Saud University.

Production and hosting by Elsevier

https://doi.org/10.1016/j.arabjc.2022.104215

mice confirmed that EOAPA can effectively prevent mouse death by downregulating the levels of inflammatory factors in serum, such as IL-6, tumor necrosis factor-α (TNF-α) and interferon-γ (IFN-γ). The above results showed that there is satisfactory potential for EOAPA to be developed and applied as a natural pharmaceutical and cosmetic additive.



## 1. Introduction

Inflammation refers to the immune system's responses that defends against harmful stimuli, containing tissue infection, tissue injury, and toxins (Nathan, 2002). Normal inflammation plays a protective role in innate immune responses against interference from external microbes, while nonresolution of inflammation has been proven to lead to various diseases, including diabetes, cardiovascular disease, atherosclerosis, rheumatoid arthritis and so on (Nathan and Ding, 2010). One crucial regulator of inflammatory response is nuclear transcription factor-κB (NF-κB), which activates target genes including inducible enzymes, chemokines, as well as proinflammatory cytokines, and leads to high secretion of interleukin-6 (IL-6), monocyte chemokine-1 (MCP-1), and tumor necrosis factor-α (TNF-α), belonging to proinflammatory cytokines (Dunkhunthod et al., 2021).

Inflammation is tightly intertwined with oxidative stress (Liu et al., 2020), which can activate NF-κB signaling (Wang et al., 2014), leading by imbalance between the release of free radicals such as reactive oxygen species (ROS) and reactive nitrogen species (RNS) and antioxidants. Therefore, oxidative stress has been showed a potential adverse effect on the organism attributed to its damage of crucial biomolecules and cells (Tu et al., 2019). ROS not only plays an important role in numerous physiological functions, but also leads to various inflammatory diseases including cardiovascular disease, COVID-19, diabetes, and cancer (Barciszewska, 2021). Studies have indicated that scavenging ROS can effectively prevent NF-κB activation and inhibit the inflammatory response (Guo et al., 2014).

Chinese herbs, used in preventing and treating diseases with thousands of years, have gained more attention from world, and numerous of which have been developed into natural additives of antioxidant and anti-inflammatory functional foods with low adverse side effects. *Atractylodes macrocephala* Koidz. (AM) belonging to the genus Atractylodes in the largest Compositae family, has been distributed throughout the tropical and subtropical regions for more than 700 years (Zhu et al., 2018). The rhizome of AM, called bai-zhu, clinically used for thousands of years, has been reported that it possesses a variety of pharmacological activities, such as improving gastrointestinal function (Xiang et al., 2020), anti-tumor, anti-inflammatory (Bailly, 2021), and anti-oxidative activities. AM has been not only approved as a functional food in China, but also broadly used in Japanese and Korean traditional medicine with long history.

Essential oil is a natural volatile produced by plants with important application value in the food, cosmetics, perfume, and pharmaceutical industries. Essential oil derived from the rhizome of AM has proved its ability in significant anti-inflammatory, anti-oxidant, and neuroprotective activities, which mainly contains atractylone, *β*-eudesmol, thymol, hinesol, atractylenolide I-IV (Wu et al., 2020). Therefore, there is significant medicinal value in the essential oil from the rhizome of AM.

In China, it is estimated that the demand for the AM rhizome on an annual basis is approximately 7,000 tonnes. However, the aerial (aboveground) parts of AM, which account for approximately 60% of the total plant mass, has not been reasonably developed and utilized (Peng et al., 2010). Active natural compounds in the aerial parts of AM, including lupeol, *β*-amyrin, and (9*Z*,12*Z*,15*Z*)-octadeca-9,12,15-trienoic acid, have been proven to possess bioactivities containing antibacterial and antitumor activities (Peng et al., 2010). Therefore, as a promising choice, there is still great potential in utilization of the remaining aerial parts of the AM, and if this occurred, it would greatly support sustainable agricultural practices. However, there are no comprehensive studies have been performed based on the biological activity or constituents of the essential oil of the aerial parts of AM (EOAPA), which restrict its development. Therefore, to promote the application of EOAPA as the antioxidant and anti-inflammatory raw material, the study was conducted to characterize the constituents, investigate the antioxidant and anti-inflammatory effects, and explore the potential mechanisms of anti-inflammatory action of EOAPA.

## 2. Materials and methods

### 2.1. Reagents

Ferric chloride, gallic acid and butylated hydroxytoluene (BHT) were purchased from Bide Pharmatech ltd. (Shanghai, China). Cell counting kit-8 (CCK-8, Biosharp China), bicinchoninic acid assay kit (BCA, Beyotime, Shanghai, China), 2,7-dichlorodi-hydrofluorescein diacetate (DCFH-DA), Folin-Ciocalteu phenol reagent, 4′,6-diamidino-2-phenylindole (DAPI) and 2,3,5-triphenyltetrazolium chloride (TPTZ) were obtained from Macklin Biochemical Co., ltd. (Shanghai, China). 1,1-Diphenyl-2-picrylhydrazyl (DPPH) and lipopolysaccharide (LPS) were derived from Sigma-Aldrich (St. Louis, MO, USA). Anti-p65 (ab32536), anti-iNOS (ab178945), anti-COX2 (ab179800) antibodies and Alexa Fluor® 488-labeled secondary antibody (ab150073) were purchased from Abcam (Cambridge, MA, USA). Anti-β-actin (4970S) antibody (CST, Danvers, MA, USA) and BD Cytometric Bead Array (CBA) mouse inflammation kit (BD Biosciences, San Diego, EE. UU).

### 2.2. Plant materials and essential oil preparation

In November 2021, fresh aerial parts of cultivated AM were collected at Lishui (Zhejiang, China) (27°61′N, 119°06′E). After being authenticated by Prof. Zhishan Ding of Zhejiang Chinese Medical University in China, the plant materials were air-dried in the shade. A voucher specimen (No. AM20211112) was deposited at the Academy of Chinese Medical Sciences, Zhejiang Chinese Medical University.

First, 600 g of dried powdered aerial parts of AM was suspended in 3 L water, and submitted to simultaneous distillation extraction (SDE) using a classical Likens-Nickerson apparatus for 4 h with 100 mL of dichloromethane. Then, the extract was concentrated at 25°C under reduced pressure, after dried with anhydrous magnesium sulfate, and a canary yellow EOAPA was then obtained.

### 2.3. Animals

Male C57BL/6 mice (aged 9–12 weeks, 19–22 g) and commercial pelleted feed were supplied by the Laboratory Animal

Research Center of Zhejiang Chinese Medical University (Hangzhou, Zhejiang Province, China). The animals were maintained on a 12-hour light/dark cycle, at 25 °C and 40%–60% humidity, and fed with normal diet. The experiments carried on were approved by the Animal Ethical Committee of Zhejiang Chinese Medical University (IACUC-20220314–17).

### 2.4. Gas chromatography-quadrupole-time of flight-mass spectrometry (GC-Q/TOF-MS) analysis of essential oil components

The EOAPA components were characterized by an Agilent Technologies 7890B GC system (Agilent Technologies, MA, USA) equipped with an HP-5 MS capillary column (30 m × 0.25 mm × 0.25 μm), combined with an Agilent 7250 time-of-flight mass spectrometer (Agilent Technologies, MA, USA) using helium as carrier gas (flow rate, 1.0 mL/min). The initial temperature was kept at 50°C during 3 min, increased by 5°C/min to 280°C, and then held for 5 min. The ion source and injector temperature were maintained at 250°C. The mass spectra were operated using 70 eV of electron energy in the scan range of $m/z$ 40–450. Then, 1 μL of the sample (diluted with ethyl acetate) was injected at a split ratio of 10:1. The retention indices (RI) of the EOAPA components were characterized using a $C_7$–$C_{40}$ *n*-alkane series. The identification of the components was performed by the comparison of the retention indices and mass spectra from the NIST library (NIST 14).

### 2.5. Assay of total phenolic content

The Folin-Ciocalteu method was conducted to characterize the total phenolic content in EOAPA (Hazrati et al., 2020). In brief, 100 μL of EOAPA (1.25 mg/mL in 50% ethanol) was added to 60 μL of Folin-Ciocalteu reagent. After 3 min of incubation, 60 μL of 10% sodium carbonate was added. After 1 h of incubation in dark, the absorbance was recorded at the wavelength of 765 nm using a standard curve obtained with a series of concentrations of gallic acid.

### 2.6. Assay of antioxidants

#### 2.6.1. DPPH$^\bullet$ radical scavenging activity

The DPPH$^\bullet$ test was conducted following the procedure of Hazrati et al. (Hazrati et al., 2019) with slight modification. Briefly, 100 μL of diluted EOAPA was added to 100 μL of DPPH$^\bullet$ solution in ethanol (0.1 mM) and incubated in dark for 30 min before measuring the absorbance at 517 nm. BHT was used as a positive control.

#### 2.6.2. ABTS$^{\bullet+}$ radical scavenging activity

The ABTS$^{\bullet+}$ test of EOAPA was adapted from Srećković et al. (Srećković et al., 2020) compared with a positive control (BHT). In short, 180 μL of newly prepared ABTS$^{\bullet+}$ solution was mixed with 20 μL of different concentrations of EOAPA. After 6 min, the values of absorbance were determined at 734 nm.

#### 2.6.3. Ferric reducing antioxidant power (FRAP) assay

FRAP assay was carried out as reported by Yosr et al. (Yosr et al., 2018). The reagent of FRAP was freshly prepared by mixing 1 mL of TPTZ (10 mM) solution in HCl (40 mM), 1 mL of ferric chloride solution (20 mM), and 10 mL of acetate buffer (300 mM, pH = 3.6). Then, 180 μL of FRAP solution was reacted with 20 μL of different concentrations of EOAPA for 6 min. The absorbance value of 593 nm was measured on a Multimode Plate Reader (EnSpire, PerkinElmer, USA).

### 2.7. Anti-inflammatory effects of EOAPA on LPS-induced RAW264.7 cells

#### 2.7.1. Cytotoxicity analysis

The cytotoxic effect of EOAPA in vitro against RAW264.7 cells (American Type Culture Collection) was evaluated using CCK-8 assay. EOAPA was dissolved in DMSO and diluted into a series of concentrations with culture medium (the final concentration of DMSO was 0.2%). RAW264.7 cells were inoculated into 96-well plates at a density of 8,000 cells per well, and then treated with various concentrations of EOAPA or vehicle (medium containing 0.2% DMSO) for 1 h, followed by the presence or absence of LPS (100 ng/mL) for the next 24 h. Furtherly, 10 μL of CCK-8 reagent was added and incubated for another 3 h, and the absorbance values of solution at 450 nm were determined using a Multimode Plate Reader (EnSpire, PerkinElmer, USA).

#### 2.7.2. Cytokine and nitric oxide (NO) levels in supernatants

RAW264.7 cells were seeded into 96-well plates at a density of $8 \times 10^4$ cells/mL. After 12 h incubation, various concentrations of EOAPA (0–40 μg/mL) were added and incubated for 1 h. Afterwards, LPS (100 ng/mL) was added and incubated for another 24 h. The supernatants of cells were collected for measurement of inflammatory cytokines and NO levels. The IL-6 and MCP-1 levels in the supernatants were analyzed by the cytometric bead array (CBA) method (Jiang et al., 2019). The NO concentrations were determined using the Griess reagent method (Brindisi et al., 2020).

#### 2.7.3. Determination of intracellular ROS

RAW264.7 cells ($8 \times 10^4$ cells/mL) were seeded into 96-well (100 μL/well) and 6-well (2 mL/well) plates, and treated according to the above assay. After a 24 h treatment, cells were stained with DCFH-DA (10 Mm) for 30 min at 37°C. The cells were gently rinsed thrice with serum-free Dulbecco's modified Eagle's medium (DMEM) to remove free EOAPA. The cells in 96-well plates were photographed using the ImageXpress Micro XLS system (Molecular Devices LLC, CA, USA). Cells in 6-well plates were collected, resuspended in phosphate-buffered saline (PBS), and then immediately analyzed using a Beckman Cytoflex S flow cytometer (Beckman Coulter, Brea, CA, USA).

### 2.8. Immunofluorescent analysis

The immunofluorescence method was performed to analyze the nuclear translocation of NF-Kb p65 as we previously reported (Jiang et al., 2019) with modification. Briefly, RAW264.7 cells were treated with various concentrations of EOAPA. After 1 h, 100 ng/mL LPS was added into cell culture for another 45 min. Fixed cells were incubated with a p65-specific antibody (1:100 dilution in PBS) at 4°C overnight

firstly and further incubated with an Alexa Fluor® 488-labeled secondary antibody (1:600 dilution in PBS, ab150073, Abcam) for 2 h. After re-stained with DAPI (10 μg/mL) for 10 min, cells were photographed using an ImageXpress Micro XLS system (Molecular Devices LLC, CA, USA).

### 2.9. RNA extraction and quantitative Real-Time polymerase chain reaction (qRT-PCR)

Total RNA from the cells was extracted using TRIzol (Invitrogen) according to the manufacturer's protocol and then quantified using a NanoDrop spectrophotometer (Thermo Fisher Scientific, United States). One microgram of RNA was reversely transcribed into complementary DNA (cDNA) using PrimeScript reverse transcription (RT) reagent kit with genomic DNA Eraser (Cwbio, China). qRT-PCR reactions were performed to detect iNOS and COX2 mRNA expression using SYBR Green I mix reagents (TaKaRa, China) on a 7500 Real-Time PCR System (Applied Biosystems). β-Actin was used as the internal control. Each reaction was run in triplicate. The change in gene expression was calculated with the $2^{-\Delta\Delta Ct}$ method. The details of PCR primers were described in Table 1.

### 2.10. Western blotting analysis

The total proteins of RAW264.7 cells were extracted according to the instructions of the M−PER mammalian protein extraction reagent (Thermo Fisher Scientific, Waltham, MA, USA), and protein concentrations were calculated using the CBA assay. The levels of inflammation-related proteins were determined by immunoblotting with specific antibodies and performed on a simple western system (ProteinSimple, San Jose, CA, USA) according to the manufacturer's instructions (Jiang et al., 2019). The immunoblotting bands were quantified by Compass Software V6.0 (ProteinSimple, San Jose, CA, USA).

### 2.11. Model of septic shock in mice and drug administration

Forty male mice were randomly divided into PBS, LPS, EOAPA (40 mg/kg) + LPS, and EOAPA (120 mg/kg) + L PS groups, $n = 10$. The mice in the control group and LPS group received an injection of the same volume of PBS (containing 1% Tween-80) for three days. In the EOAPA group, EOAPA was dissolved in PBS (containing 1% Tween-80) for intraperitoneal injection at a dose of 40 mg/kg/d and 120 mg/kg/d for 3 consecutive days. The septic shock model was induced by intraperitoneal injection of LPS (25 mg/kg) 1 h after the last administration. Survival rate was monitored for 72 h. Mice were bled by tail clipping at 24 h after LPS injection.

### 2.12. Plasma analysis

After centrifugated at 3,000 rpm for 10 min at 4°C, the levels of serum cytokines were analyzed by the CBA method (Jiang et al., 2019).

### 2.13. Statistical analysis

The obtained data in the current study are defined as arithmetic means ± standard deviation (SD) from at least three independent experiments. One-way ANOVA was performed to calculate the significance of the differences between the groups, and significance level was considered at $p < 0.05$.

## 3. Results

### 3.1. GC-Q/TOF-MS analysis of EOAPA

The chemical composition of EOAPA was analyzed by GC-Q/TOF-MS, as given in Table 2 and Fig. 1. Totally, 73 constituents were identified in the EOAPA, representing 94.75% of the total oil composition. The qualitative and quantitative determination of EOAPA showed that it was primarily composed of terpenes, accounting for 62.32%, of which 44.62% were oxygenated bicyclic sesquiterpenes, followed by bicyclic sesquiterpenes (13.82%), monocyclic sesquiterpenes (12.95%), oxygenated tricyclic sesquiterpenes (10.96%), tricyclic sesquiterpenes (8.42%), oxygenated monocyclic sesquiterpenes (6.71%), and a very small amount of tetracyclic sesquiterpenes (1.75%) and monoterpenes (0.77%). Aliphatic hydrocarbons were also important compounds, accounting for 24.39% of the EOAPA, and there were a very small proportion of aromatic compounds (8.04%). Hinesol (12.61%) was the dominant constituent of EOAPA, followed by β-eudesmol (11.51%), atractylone (5.8%), germacrene B (4.86%), valencene (3.57%), and α-oxobisabolene (2.71%).

### 3.2. Total phenol

The total phenol amount of EOAPA was 3.01 ± 0.06 mg gallic acid/100 g oil with a calibration curve equation of $Y = 13.077 X + 0.0113$, $R^2 = 0.9\,989$ (gallic acid), which was consistent with the above data showing that the content of terpenes was much higher than that of aromatic compounds (62.32% vs 8.04%). To our knowledge, there is no available data regarding the phenolic content of EOAPA.

### 3.3. Antioxidant activity

$DPPH^{\bullet}$, $ABTS^{\bullet+}$, and FRAP assays were conducted to assess the antioxidant activity of EOAPA considering different mech-

**Table 1** Primer sequences of various genes used for qRT-PCR analysis.

| Gene | Forward sequence (5′-3′) | Reverse sequence (5′-3′) |
|---|---|---|
| iNOS | CTTGGAGCGAGTTGTGGATTGTC | TAGGTGAGGGCTTGGCTGAGTGA |
| COX2 | AGAAGGAAATGGCTGCAGAA | GCTCGGCTTCCAGTATTGAG |
| β-actin | CGTGGGCCGCCCTAGGCACCA | TTGGCCTTAGGGTTCAGGGGGG |

**Table 2** Composition and content of EOAPA.

| Class | Component | Molecular formula | RI[a] | RI(NIST)[b] | Area% |
|---|---|---|---|---|---|
| Aliphatic compounds | | | | | **24.39** |
| Aliphatic acids | | | | | **6.89** |
| | 1,2-Benzenedicarboxylic acid, bis(2-methylpropyl) ester | $C_{16}H_{22}O_4$ | 1870 | 1870 ± 4 | 0.33 |
| | *n*-Hexadecanoic acid | $C_{16}H_{32}O_2$ | 1961 | 1968 ± 7 | 4.26 |
| | Phytol | $C_{20}H_{40}O$ | 2114 | 2114 ± 5 | 0.61 |
| | 9,12-Octadecadienoic acid *(Z,Z)*- | $C_{18}H_{32}O_2$ | 2132 | 2133 ± 12 | 0.64 |
| | 9,12,15-Octadecatrienoic acid, *(Z,Z,Z)*- | $C_{18}H_{30}O_2$ | 2138 | 2139 ± 20 | 0.57 |
| | Octadecanoic acid | $C_{18}H_{36}O_2$ | 2160 | 2172 ± 7 | 0.48 |
| Aliphatic alcohols | | | | | **5.52** |
| | 3-Hexen-1-ol, *(E)*- | $C_6H_{12}O$ | 854 | 856 ± 1 | 1.42 |
| | 1-Hexanol | $C_6H_{14}O$ | 867 | 868 ± 4 | 2.81 |
| | Heptanal | $C_7H_{14}O$ | 903 | 901 ± 2 | 0.28 |
| | 1-Octen-3-ol | $C_8H_{16}O$ | 979 | 980 ± 2 | 0.25 |
| | Pentadecanal- | $C_{15}H_{30}O$ | 1714 | 1715 ± 3 | 0.52 |
| | 1-Heneicosanol | $C_{21}H_{44}O$ | 2394 | 2380 ± 15 | 0.24 |
| Aliphatic aldehydes | | | | | **6.94** |
| | Hexanal | $C_6H_{12}O$ | 802 | 800 ± 2 | 3.06 |
| | 2-Hexenal | $C_6H_{10}O$ | 851 | 851 ± 5 | 0.76 |
| | 2-Heptenal, *(Z)*- | $C_7H_{12}O$ | 956 | 958 ± 6 | 0.21 |
| | Nonanal | $C_9H_{18}O$ | 1104 | 1104 ± 2 | 0.62 |
| | 2-Nonenal, *(E)*- | $C_9H_{16}O$ | 1160 | 1162 ± 3 | 0.32 |
| | Decanal | $C_{10}H_{20}O$ | 1206 | 1206 ± 2 | 0.53 |
| | 2,4-Decadienal, *(E,E)*- | $C_{10}H_{16}O$ | 1316 | 1317 ± 3 | 1.03 |
| | Cyclohexanebutanal, 2-methyl-3-oxo-, cis- | $C_{11}H_{18}O_2$ | 1521 | 1515 ± 6 | 0.41 |
| Aliphatic ethers | | | | | **2.91** |
| | 3,6-Dimethyl-2,3,3a,4,5,7a-hexahydrobenzofuran | $C_{10}H_{16}O$ | 1195 | 1192 | 0.32 |
| | Dihydroedulan IIA | $C_{13}H_{22}O$ | 1296 | 1293 | 0.35 |
| | Theaspirane A | $C_{13}H_{22}O$ | 1301 | 1302 ± 4 | 0.32 |
| | Tau-Cadinol acetate | $C_{17}H_{28}O_2$ | 1798 | 1805 | 1.56 |
| | Hexadecanoic acid, ethyl ester | $C_{18}H_{36}O_2$ | 1993 | 1993 ± 3 | 0.36 |
| Aliphatic ketones | | | | | **1.57** |
| | 5,9-Undecadien-2-one, 6,10-dimethyl-, *(E)*- | $C_{13}H_{22}O$ | 1454 | 1453 ± 2 | 0.33 |
| | *trans*-*β*-Ionone | $C_{13}H_{20}O$ | 1489 | 1486 ± 4 | 0.36 |
| | 2-Pentadecanone, 6,10,14-trimethyl- | $C_{18}H_{36}O$ | 1846 | 1844 ± 4 | 0.88 |
| Aliphatic hydrocarbons | | | | | **0.56** |
| | 1-Tridecyne | $C_{13}H_{24}$ | 1294 | 1297 ± 1 | 0.18 |
| | Cetene | $C_{16}H_{32}$ | 1592 | 1592 ± 1 | 0.19 |
| | 3-Octadecene, *(E)*- | $C_{18}H_{36}$ | 1792 | 1785 ± 1 | 0.19 |
| Aromatic compounds | | | | | 8.04 |
| Aromatic alcohols | | | | | **1.6** |
| | Benzyl alcohol | $C_7H_8O$ | 1034 | 1036 ± 4 | 0.33 |
| | Phenylethyl Alcohol | $C_8H_{10}O$ | 1113 | 1116 ± 5 | 0.86 |
| | Phenol, 2,5-bis(1,1-dimethylethyl)- | $C_{14}H_{22}O$ | 1513 | 1514 | 0.41 |
| Aromatic aldehydes | | | | | **1.04** |
| | Benzaldehyde | $C_7H_6O$ | 960 | 962 ± 3 | 0.24 |
| | Benzeneacetaldehyde | $C_8H_8O$ | 1043 | 1045 ± 4 | 0.8 |
| Aromatic ethers | | | | | **3.15** |
| | 3-Furaldehyde | $C_5H_4O_2$ | 832 | 833 ± 4 | 1.13 |
| | Furan, 2-pentyl- | $C_9H_{14}O$ | 992 | 993 ± 2 | 1.42 |
| | Benzofuran, 2,3-dihydro- | $C_8H_8O$ | 1219 | 1224 ± 3 | 0.6 |
| Aromatic ketones | | | | | **1.14** |
| | Ethanone, 1-(2-hydroxy-5-methylphenyl)- | $C_9H_{10}O_2$ | 1314 | 1316 | 1.14 |
| Aromatic hydrocarbons | | | | | **1.11** |
| | Ethylbenzene | $C_8H_{10}$ | 860 | 855 ± 10 | 0.3 |
| | *p*-Xylene | $C_8H_{10}$ | 868 | 865 ± 7 | 0.4 |
| | α-Curcumene | $C_{15}H_{22}$ | 1485 | 1483 ± 3 | 0.41 |
| Terpenes | | | | | **62.32** |
| monoterpenes | | | | | **0.48** |
| Oxygenated acyclic monoterpenes | | | | | **0.48** |
| | Linalool | $C_{10}H_{18}O$ | 1100 | 1099 ± 2 | 0.48 |
| Sesquiterpenes | | | | | **61.84** |

(*continued on next page*)

**Table 2** (*continued*)

| Class | Component | Molecular formula | RI[a] | RI(NIST)[b] | Area% |
|---|---|---|---|---|---|
| Monocyclic sesquiterpenes | | | | | **12.25** |
| | Humulene | $C_{15}H_{24}$ | 1458 | 1454 ± 3 | 0.85 |
| | γ-Curcumene | $C_{15}H_{24}$ | 1482 | 1480 ± 2 | 0.66 |
| | β-Sesquiphellandrene | $C_{15}H_{24}$ | 1527 | 1524 ± 2 | 1.7 |
| | Elemol | $C_{15}H_{26}O$ | 1553 | 1549 ± 2 | 1.27 |
| | Germacrene B | $C_{15}H_{24}$ | 1562 | 1557 ± 3 | 4.86 |
| | Zingiberenol | $C_{15}H_{26}O$ | 1617 | 1616 ± 5 | 0.2 |
| | α-Oxobisabolene | $C_{15}H_{24}O$ | 1750 | 1750 | 2.71 |
| Bicyclic sesquiterpenes | | | | | **36.42** |
| | Caryophyllene | $C_{15}H_{24}$ | 1424 | 1419 ± 3 | 1.76 |
| | Alloaromadendrene | $C_{15}H_{24}$ | 1467 | 1461 ± 2 | 0.29 |
| | β-Selinene | $C_{15}H_{24}$ | 1491 | 1486 ± 3 | 1.53 |
| | 7-*epi*-Sesquithujene | $C_{15}H_{24}$ | 1497 | 1391 ± 2 | 0.93 |
| | Cashmeran | $C_{15}H_{22}O$ | 1513 | 1508 ± 5 | 0.59 |
| | γ-Cadinene | $C_{15}H_{24}$ | 1518 | 1513 ± 2 | 0.53 |
| | (4aR,8aS)-4a-Methyl-1-methylene-7-(propan-2-ylidene) decahydronaphthalene | $C_{15}H_{24}$ | 1540 | 1544 | 3.57 |
| | 4a,5-Dimethyl-3-(prop-1-en-2-yl)-1,2,3,4,4a,5,6,7-octahydronaphthalen-1-ol | $C_{15}H_{24}O$ | 1550 | 1553 | 0.45 |
| | γ-Eudesmol | $C_{15}H_{26}O$ | 1635 | 1631 ± 1 | 1.86 |
| | Hinesol | $C_{15}H_{26}O$ | 1645 | 1645 ± 3 | 12.61 |
| | β-Eudesmol | $C_{15}H_{26}O$ | 1656 | 1649 ± 2 | 11.51 |
| | Guai-1(10)-en-11-ol | $C_{15}H_{26}O$ | 1671 | 1667 ± 2 | 0.79 |
| Tricyclic sesquiterpenes | | | | | **12.08** |
| | 7-*epi*-Silphiperfol-5-ene | $C_{15}H_{24}$ | 1347 | 1348 | 0.55 |
| | Modephene | $C_{15}H_{24}$ | 1384 | 1385 ± 0 | 1.03 |
| | Berkheyaradulene | $C_{15}H_{24}$ | 1390 | 1386 ± 6 | 1.77 |
| | β-Maaliene | $C_{15}H_{24}$ | 1404 | 1405 ± 16 | 0.48 |
| | β-Isocomene | $C_{15}H_{24}$ | 1411 | 1412 ± 0 | 1.42 |
| | Caryophyllene oxide | $C_{15}H_{24}O$ | 1589 | 1581 ± 2 | 0.26 |
| | Epiglobulol | $C_{15}H_{26}O$ | 1597 | 1585 ± 5 | 0.51 |
| | Atractylone | $C_{15}H_{20}O$ | 1663 | 1662 ± 9 | 5.8 |
| | Cedr-8-en-13-ol | $C_{15}H_{24}O$ | 1691 | 1688 ± 1 | 0.26 |
| Tetracyclic sesquiterpenes | | | | | **1.09** |
| | Ledene-oxide-Ⅱ | $C_{15}H_{24}O$ | 1632 | 1631 | 1.09 |

(a) Retention indices experimentally calculated based on the $C_7$-$C_{40}$ *n*-alkanes standard, (b) Retention indices were taken from NIST GC-RI database.

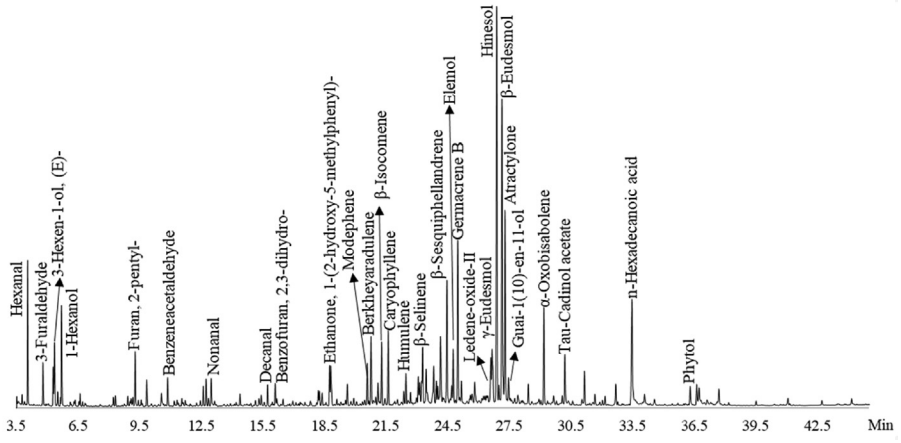


**Fig. 1** Total ion current chromatogram of EOAPA by GC-Q/TOF-MS.

anisms. As depicted in Fig. 2, EOAPA characterized significant antioxidant properties in a dose-dependent manner in the concentration range of 0.625 mg/mL to 10 mg/mL. However, its $IC_{50}$ value for $DPPH^{\bullet}$ and $ABTS^{\bullet+}$ radicals and $OD_{0.5}$ for iron ion reduction (3.113 ± 0.037 mg/mL, 4.837 ± 0.169 mg/mL, and 3.978 ± 0.258 mg/mL, respectively) were significantly higher than those of positive control BHT (12.257 ± 0.136 μg/mL, 35.697 ± 0.860 μg/mL, and 35.397 ± 0.580 μg/mL, respectively), indicating that the direct antioxidant capacity of EOAPA was weak. Reports have shown that the

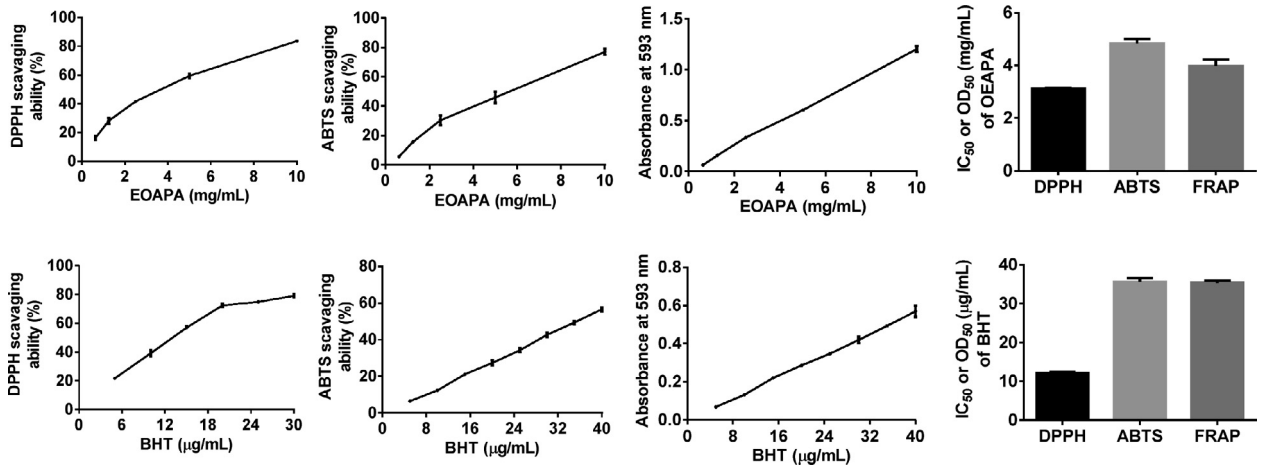


**Fig. 2** Antioxidant activity of the EOAPA in DPPH•, ABTS•$^{+}$ and FRAP assay.

total phenol was closely related to the antioxidant capacity (Akgün et al., 2021), while the EOAPA was abundant in non-phenolic components, which were proved to be poor antioxidant.

### *3.4. Cytotoxic effect of EOAPA on RAW264.7 cells*

The cytotoxicity of EOAPA on RAW264.7 cells was evaluated by CCK-8 assay. The results revealed that treatments with 5–40 μg/mL of EOAPA did not cause distinct cytotoxicity, regardless of the presence or absence of LPS (100 ng/mL) (Fig. 3A). Therefore, concentrations within 40 μg/mL of EOAPA were chosen for further exploration of anti-inflammatory and anti-oxidant effects and potential mechanism.

### *3.5. Anti-inflammatory effects on LPS-induced RAW264.7 cells*

#### *3.5.1. EOAPA inhibits the secretion of IL-6 and MCP-1 in a dose-dependent manner*

Molecular components of pathogens such as LPS can activate macrophages to secrete cytokines and mediate the inflammatory response. As shown in Fig. 3, LPS stimulation dramatically increased the cytokine levels of IL-6, TNF-α and MCP-1, while pretreatment with different concentrations of EOAPA significantly decreased the secretion of MCP-1 and IL-6 in a dose-dependent manner (Fig. 3B, C). As displayed in Fig. 3, there was significant inhibition of MCP-1 and IL-6 by EOAPA, with inhibition rates reaching 38.997 ± 1.339% and 32.822 ± 1.766%, respectively, at 2.5 μg/mL of EOAPA treatment, and $IC_{50}$ values of 3.52 ± 0.56 μg/mL and 5.35 ± 0.82 μg/mL, respectively. However, EOAPA could not effectively downregulate TNF-α levels (Fig. 3D).

#### *3.5.2. EOAPA attenuates inducible nitric oxide synthase (iNOS) and cyclooxygenase-2 (COX-2) expression*

LPS stimulated macrophages to secrete TNF-α, IL-6, and MCP-1, and also promoted the expression of iNOS and COX-2 genes to release inflammatory mediators including prostaglandin E2 (PGE2) and nitric oxide (NO), and aggravate the inflammatory response (Yao et al., 2018). To investigate whether EOAPA can inhibit the expression of iNOS and COX-2, quantitative Real-time PCR (qRT-PCR) and western blot analysis were performed.

The data revealed dramatic overexpression of iNOS and COX-2 mRNA and proteins induced by LPS in RAW264.7 macrophages compared to unchallenged cells (Fig. 4). As expected, EOAPA at all pretreated concentrations significantly downregulated LPS-induced iNOS and COX-2 mRNA levels compared to LPS-treated cells (Fig. 4A, B). For protein levels, compared with the LPS-stimulated group, there was no significant downregulation of iNOS and COX-2 by EOAPA at 5 μg/mL, and in other treatment groups, there was a remarkable decrease in the protein levels of iNOS and COX-2 (Fig. 4C, D).

#### *3.5.3. EOAPA exerts anti-inflammatory activity by inhibiting NF-κB p65 nuclear translocation*

The activated NF-κB p65 protein can control the expression of numerous inflammatory genes, such as TNF-α, IL-6, MCP-1, iNOS, and COX-2. Therefore, western blotting was conducted to determine the level of p65 protein in nuclei. As shown in Fig. 5A, LPS significantly increased the level of p65 in the nucleus, while EOAPA pretreatment dramatically attenuated LPS-induced p65 nuclear translocation in a dose-dependent manner, which was further reconfirmed by immunofluorescence assay, as shown in Fig. 5B. Based on these data, it was observed that EOAPA inhibits NF-κB p65 nuclear translocation, which further inhibits the expression of target inflammatory genes.

### *3.6. ROS production inhibition by EOAPA in LPS-induced RAW264.7 cells*

Based on the inhibitory effect of EOAPA on NF-κB and related inflammatory genes, we speculated that EOAPA may exert its anti-inflammatory activity by inhibiting the production of ROS induced by LPS. To verify the speculation, the levels of ROS were measured. As expected, flow cytometric analysis indicated that LPS exposure dramatically increased intracellular ROS. On the contrary, EOAPA pretreatments effectively downregulated the production of ROS in a dose-dependent manner (Fig. 6A), which was confirmed by fluorescence microscopy analysis (Fig. 6B).

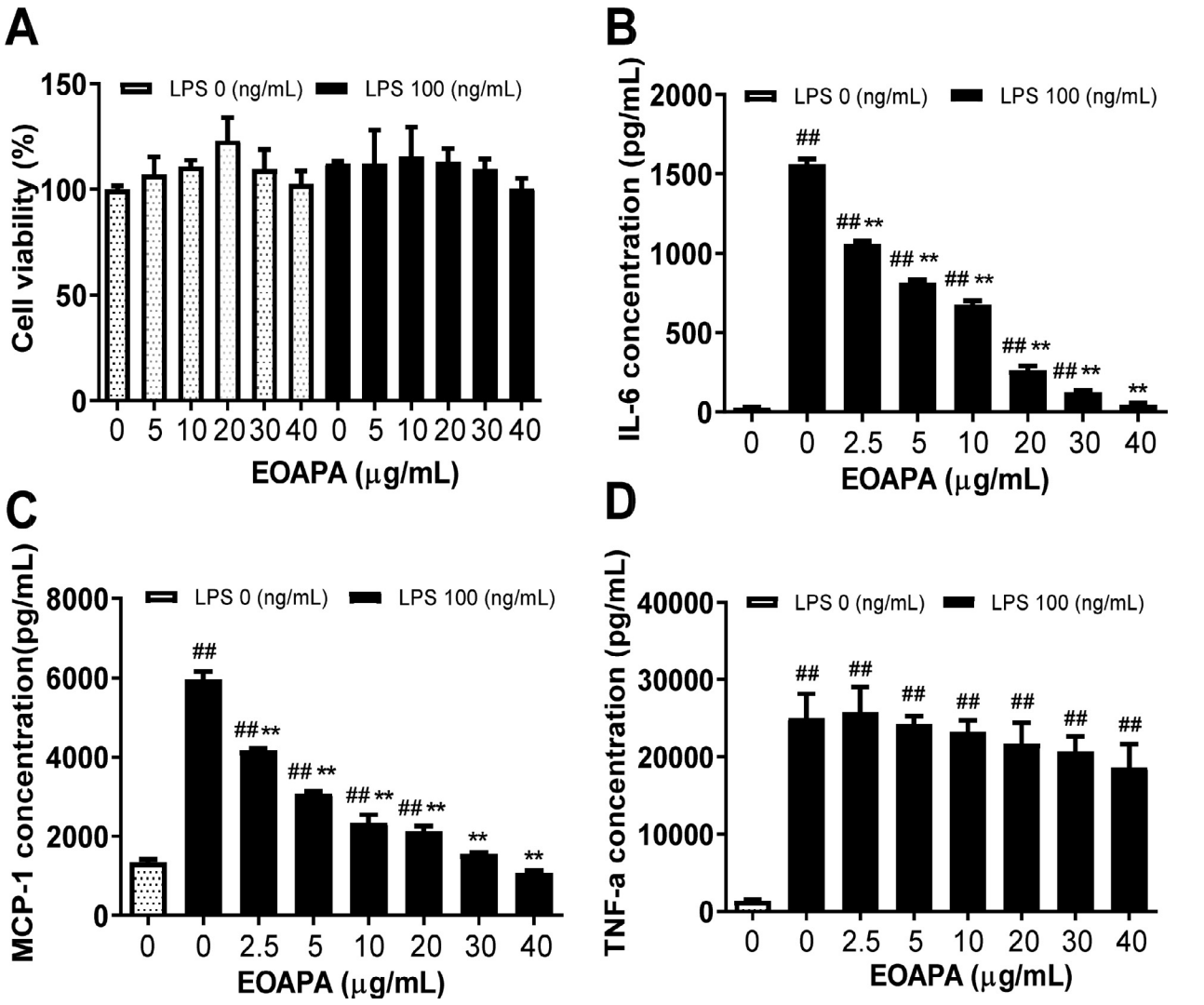


**Fig. 3** Evaluation of anti-inflammatory of EOAPA in LPS-stimulated RAW264.7 cells. (A) Effect of EOAPA on cell viability of RAW264.7 cells was estimated by CCK-8 assay. (B) IL-6 and (C) MCP-1 levels in culture supernatant pre-treated by different concentrations of EOAPA. Data represent Mean ± SD ($n = 3$). $^{\#\#}$ $p < 0.01$ versus control group (treated by reagent); $^{**}$ $p < 0.01$ versus LPS treated group.

In addition to ROS, RNS is also a vital factor leading to cellular oxidative stress. NO, as a multi-effector molecule, can also be rapidly oxidized by ROS to RNS, which is closely related to inflammation. It is well known that LPS can induce macrophages to overexpress iNOS, resulting in a large amount of NO release (Reuter et al., 2010). The above data showed that EOAPA significantly inhibited the expression of iNOS induced by LPS. Therefore, the level of NO in the cell culture supernatant was determined. Consistently, compared to LPS-exposed group, EOAPA pretreatment dose-dependently decreased the NO level (Fig. 6C). Compared with the weak antioxidant activity based on chemical reaction in vitro, EOAPA exhibited a more significant free radical scavenging activity against LPS-induced excess ROS and RNS at the cellular level. Therefore, further research is needed to uncover the potential mechanism of EOAPA.

### *3.7. EOAPA reduced septic death and inflammatory cytokine production in an LPS-induced septic model*

Based on the above findings that EOAPA blocked LPS-induced macrophage activation, we then hypothesized that EOAPA possessed the ability to inhibit LPS-induced immune responses in vivo. To verify this, a model of septic shock was established in male C57BL/6 mice by intraperitoneal injection of LPS (Fig. 7A). As shown in Fig. 7B, the survival rate of LPS group was 40%, whereas EOAPA increased the survival rate to 60% at 40 mg/kg and 80% at 120 mg/kg.

Next, to examine the effect of EOAPA on the production of inflammatory cytokines in an LPS-induced septic model, the CBA method was performed. As expected, the levels of IL-6 dramatically increased in response to LPS stimulation, which was remarkably downregulated by EOAPA pretreatment

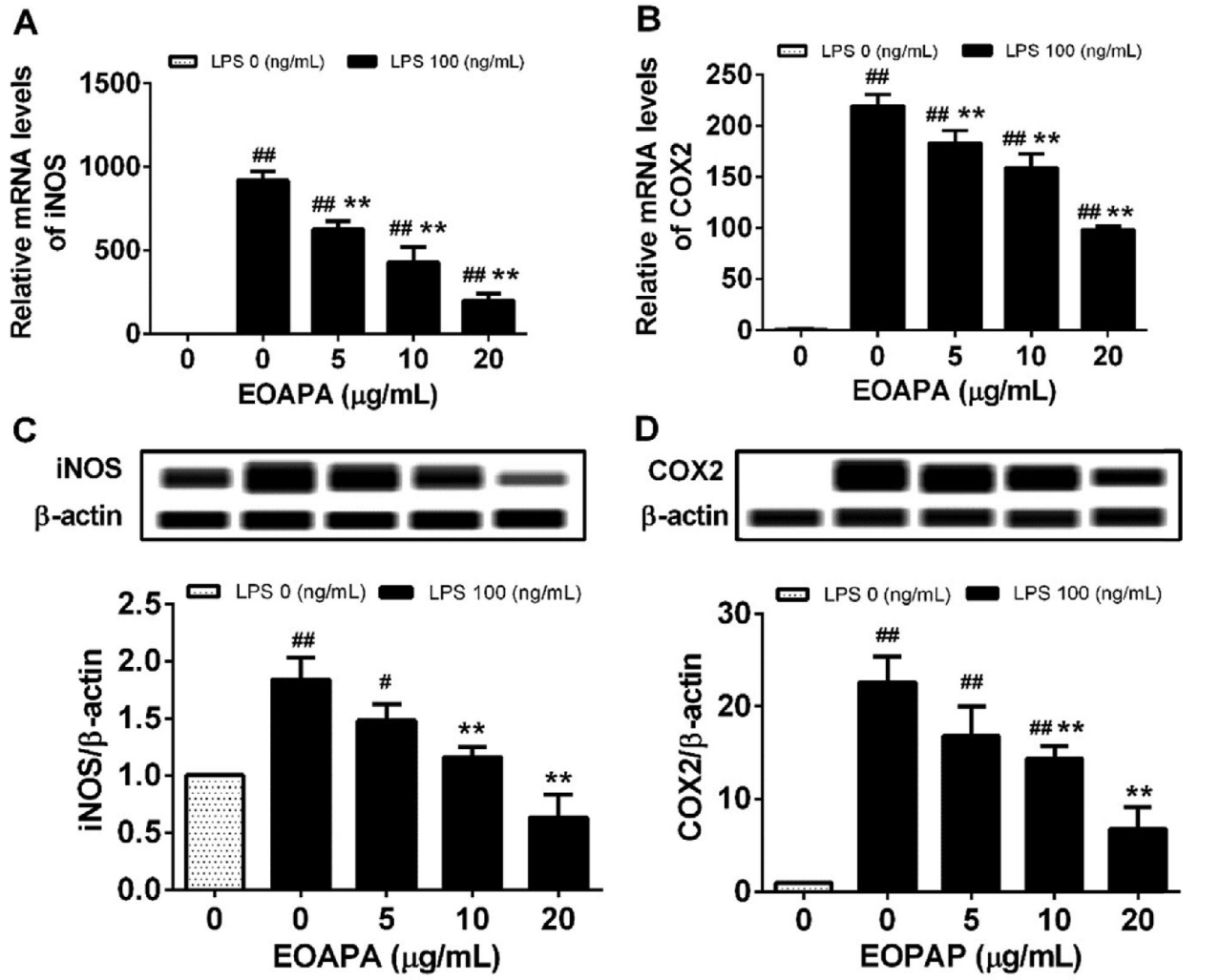


**Fig. 4** Effects of EOAPA on overexpression of (A) iNOS and (B) COX-2 genes and (C) iNOS and (D) COX-2 proteins. Cells were treated with increasing concentrations of EOAPA for 1 h and with LPS (100 ng/mL). The expression of iNOS and COX-2 genes were determined by qRT-PCR after treated with LPS for 6 h. While, the expression of iNOS and COX-2 proteins were analyzed using simple western immunoblotting after treated with LPS for 24 h. Data represent Mean ± SD ($n = 3$). $^{\#}p < 0.05$, $^{\#\#}p < 0.01$ versus control group (treated by reagent); $^{**}p < 0.01$ versus LPS treated group.

(Fig. 7C). Consistently, LPS stimulation promoted the production of TNF-α, IFN-γ and IL-10, while pre-administration of EOAPA (120 mg/kg) reduced the corresponding inflammatory cytokines (Fig. 7D–F). However, EOAPA at 40 mg/kg could not effectively downregulate TNF-α or IL-10 levels. These results confirmed that EOAPA prevented LPS-induced septic shock by alleviation of inflammatory responses in vivo.

## 4. Discussion

Previous studies have described that the rhizome oil of AM included atractylone, β-eudesmol, germacrene B and valencene. Although the constituents in rhizome oil vary with different origins (Guo et al., 2021), the rhizome oil component present in the highest quantity was atractylone, accounting for 40–70%, which is more than 7 times the amount found in the aerial parts oil (Gu et al., 2019). Compared with rhizome oil, there were more abundant components in the aerial parts oil in addition to the main common components of hinesol, β-eudesmol, atractylone, and germacrene B. Hinesol is the dominant component of the aerial parts oil, but the amount reported in the rhizome oil of AM is low (Wu et al., 2020). Hinesol exerts the most promising anticancer activity by downregulating NF-κB and MEK/ERK pathways to induce apoptosis and reduce cell growth (Guo et al., 2019). β-Eudesmol, main constituents of EOAPA, has been developed into a novel agent of cosmetics as well as medicine and pharmacy attributed to the function of anti-inflammatory and antioxidant via NF-κB signaling pathway (Han et al., 2017). Similarly, atractylone could block NF-κB signaling pathway and mitigate inflammatory conditions (Kim et al., 2016). Based on these, we surmised EOAPA had advantageous potential in antioxidation and anti-inflammation and furtherly, would develop into a natural additive of antioxidant and anti-inflammatory functional food.

LPS, a glycan, consisted of O-antigen, core sugars and lipid A, which is termed as pathogen associated molecular patterns

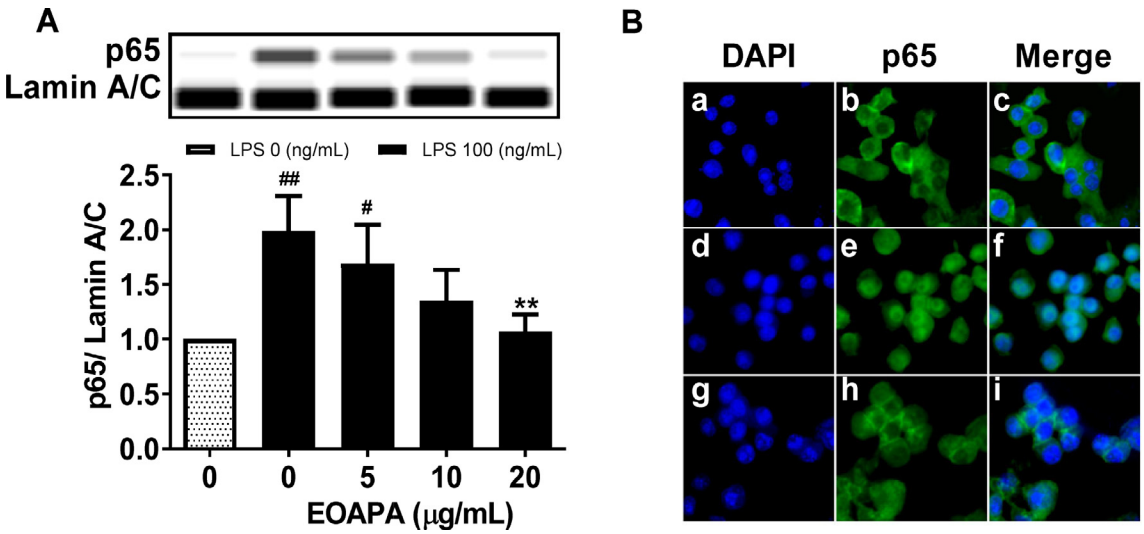


**Fig. 5** Effects of EOAPA on NF-κB p65 nuclear translocation. RAW264.7 cells were pre-treated with various concentrations of EOAPA for 1 h, and then LPS-stimulated during 1 h. (A) The content of p65 in the nucleus was determined by simple western immunoblotting. (B) Cells were fixed, permeabilized and conducted immunofluorescence assay. a–c control group, d–f LPS induced group, g–i 20 μg/mL EOAPA pre-treated and then LPS induced group. Data represent Mean ± SD ($n = 3$). $^{\#}p < 0.05$, $^{\#\#}p < 0.01$ versus control group; $^{**}p < 0.01$ versus LPS group.

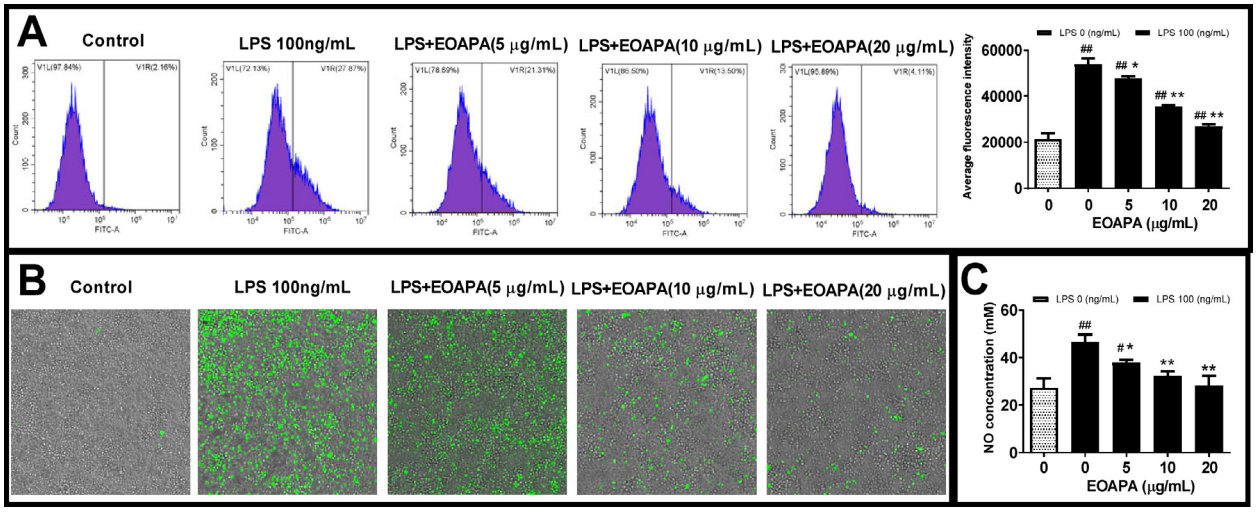


**Fig. 6** Evaluation of EOAPA on LPS induced cell oxidative stress. RAW264.7 cells were pre-treated with various concentrations of EOAPA for 1 h, and then LPS-stimulated during 24 h. Intracellular ROS was (A) recorded by flow cytometer and (B) photographed on an ImageXpress Micro Confocal High-Content Imaging System. (C) NO concentrations were measured using Griess reagent method. Data represent Mean ± SD ($n = 3$). $^{\#}p < 0.05$, $^{\#\#}p < 0.01$ versus control group; $^{*}p < 0.05$, $^{**}p < 0.01$ versus LPS group.

(PAMP), prompts innate immunity by engagement of Toll-like receptor 4 (TLR4) /myeloid differentiation-2 (MD-2) /LPS complexes (Zamyatina and Heine, 2020). With cooperation of transfer to cluster of differentiation-14 (CD14) and LPS-binding protein (LBP), LPS is presented to MD-2 and associated to TLR4. Subsequently, adapter molecules such as myeloid differentiation factor (MyD)88, TIR-containing adapter molecule (TRIF) and TRIF-related adapter are recruited, resulting in the activation of different communication signals such as NF-κB and MAPK (Neuder et al., 2009) and increasing transcription of a series of chemokines and cytokines containing MCP-1, IL-6, IL-1β and TNF-α for the mediation of the inflammatory response (Zamyatina and Heine, 2020). Excessive stimulation of LPS can lead to various disease including septic shock (Oh et al., 2019), chronic obstructive pulmonary, etc. NF-κB is a proinflammatory transcription factor acting importantly to regulate inflammatory response (Hayden and Ghosh, 2008), which is divided into five subunits: RelA/p65, p50, p52, c-Rel and RelB, sharing their Rel homology domain (RHD) responsible for DNA binding (Hayden and Ghosh, 2008). Activated NF-κB increases the expression of numerous inflammatory genes containing iNOS, COX-2, IL-1, IL-6 and TNF-α (Kumar et al., 2021).

The study of EOAPA was performed to develop a new LPS immune adjuvant or antagonists. EOAPA research into the function and regulation of the LPS-induced inflammatory pro-

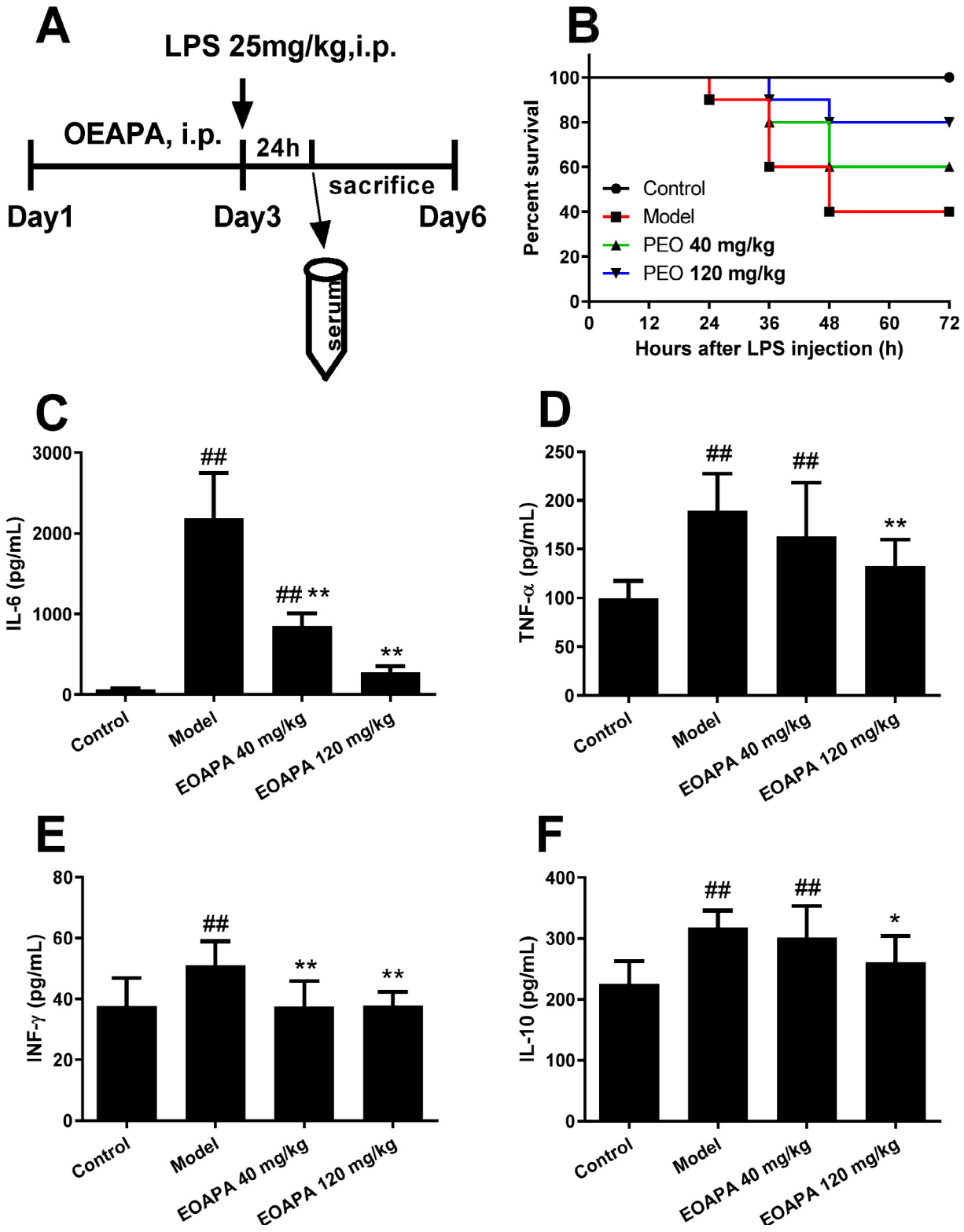


**Fig. 7** EOAPA prevented septic death and downregulated inflammatory cytokines level in LPS-induced septic shock mouse model. (A) Timetable of the LPS-induced septic shock mouse model. (B) Mice survival rate after 72-h post-LPS challenge (i.p., 25 mg/kg) with or without pre-administration of EOAPA (40 or 120 mg/kg) ($n = 10$/group). Serum levels of (C) IL-6, (D) TNF-α, (E) IFN-γ and (F) IL-10 24 h after the administration of LPS with or without pre-administration of EOAPA. Data represent Mean ± SD ($n = 10$). $^{\#}p < 0.05$, $^{\#\#}p < 0.01$ versus control group; $^{*}p < 0.05$, $^{**}p < 0.01$ versus model group.

vided evidence that EOAPA inhibited NF-κB p65 nuclear translocation used western blotting, further confirmed by immunofluorescence assay, and subsequently attenuated expression of iNOS and COX-2. Results from vitro and vivo studies using LPS induced Raw264.7 and septic shock mouse model, showed that EOAPA inhibited dramatically the secretion of IL-6 in vitro and in vivo, respectively, and decreased TNF-α levels in vivo but not effectively in vitro. In conclusion, the suppression of the NF-κB pathway of EOAPA played primary role in the inhibition on the inflammatory response and septic shock by LPS. Therefore, advances in understanding how the EOAPA inhibited NF-κB p65 nuclear translocation piqued our interests.

It is well known that the production of ROS constitutively increases in LPS-induced RAW264.7 cells (More and Makola, 2020). Numerous considerable studies have been carried out to show NF-κB activation not only relies on the classical pathway induced by immunity mediators also ROS, such as $H_2O_2$, singlet oxygen and hypochlorous acid (Gloire et al., 2006). Studies have indicated that scavenging ROS can effectively prevent NF-κB activation (Nishanth et al., 2011), which subsequently inhibits the inflammatory response. EOAPA showed significant free radical scavenging activity against LPS-induced excess ROS at the cellular level measured by flow cytometer and photographed. Overall, the EOAPA inhibition of NF-κB p65 nuclear translocation may be related to its strong ROS-scavenging ability, and the molecular mechanism of EOAPA inhibitory action on ROS-mediated NF-κB activation requires further investigation in the future.

## 5. Conclusions

Seventy-three compounds from EOAPA were identified by GC–MS, and the main compounds were hinesol, β-eudesmol, atractylone, germacrene B, and valencene. EOAPA inhibited NF-κB p65 nuclear translocation, which may be related to its strong ROS-scavenging ability against LPS challenge, thereby downregulating the expression of pro-inflammatory enzymes (iNOS and COX-2) and cytokines (MCP-1 and IL-6). Most importantly, in vivo experiments, it was confirmed that EOAPA also effectively decreased LPS-induced septic shock death by decreasing the levels of serum inflammatory cytokines such as IL-6, TNF-α, and INF-γ. These results indicated that EOAPA might be used as a natural antioxidant and anti-inflammatory agent, and it exhibited potential value for application in pharmaceutical industries.

## Funding

The present research was carried out with the financial support of the Natural Science Foundation of Zhejiang Province (No. LQ20H270008) and Science Foundation of Zhejiang Chinese Medical University (Project NOs. 2020ZG31 and 2020ZG35).

## Declaration of Competing Interest

The authors declare that they have no known competing financial interests or personal relationships that could have appeared to influence the work reported in this paper.

## Acknowledgements

We thank LetPub (www.letpub.com) for its linguistic assistance during the preparation of this manuscript.

## References

Akgün, N., Çelik, Ö.F., Kelebekli, L., 2021. Physicochemical properties, total phenolic content, and antioxidant activity of chestnut, rhododendron, acacia and multifloral honey. J. Food Meas. Charact. 15, 3501–3508. https://doi.org/10.1007/s11694-021-00937-3.

Bailly, C., 2021. Atractylenolides, essential components of Atractylodes-based traditional herbal medicines: antioxidant, anti-inflammatory and anticancer properties. Eur. J. Pharmacol. 891,. https://doi.org/10.1016/j.ejphar.2020.173735 173735.

Barciszewska, A.M., 2021. Elucidating of oxidative distress in COVID-19 and methods of its prevention. Chem. Biol. Interact. 344,. https://doi.org/10.1016/j.cbi.2021.109501 109501.

Brindisi, M.C., Bouzidi, L., Frattaruolo, L., et al, 2020. Chemical Profile, Antioxidant, Anti-Inflammatory, and Anti-Cancer Effects of Italian *Salvia rosmarinus* Spenn. Methanol Leaves Extracts. Antioxidants (Basel) 9, 826–846. https://doi.org/10.3390/antiox9090826.

Dunkhunthod, B., Talabnin, C., Murphy, M., et al., 2021. *Gymnema inodorum* (Lour.) Decne. Extract Alleviates Oxidative Stress and Inflammatory Mediators Produced by RAW264.7 Macrophages. Oxid. Med. Cell. Longev. 2021, 8658314. https://doi.org/10.1155/2021/8658314.

Gloire, G., Legrand-Poels, S., Piette, J., 2006. NF-kappaB activation by reactive oxygen species: fifteen years later. Biochem. Pharmacol. 72, 1493–1505. https://doi.org/10.1016/j.bcp.2006.04.011.

Gu, S., Li, L., Huang, H., et al, 2019. Antitumor, Antiviral, and Anti-Inflammatory Efficacy of Essential Oils from *Atractylodes macrocephala* Koidz. produced with different processing methods. Molecules 24, 2956–2969. https://doi.org/10.3390/molecules24162956.

Guo, W.Q., Liu, S.B., Ju, X., et al, 2019. The antitumor effect of hinesol, extract from *Atractylodes lancea* (Thunb.) DC. by proliferation, inhibition, and apoptosis induction via MEK/ERK and NF-kappaB pathway in non-small cell lung cancer cell lines A549 and NCI-H1299. J. Cell. Biochem. 120, 18600–18607. https://doi.org/10.1002/jcb.28696.

Guo, H., Xu, M.T., Wu, Z.F., et al, 2021. Drying kinetics and the variation of volatile components of *Atractylodes macrocephala* during hot-air drying process. China. J. Chin. Mater. Med. 47, 922–930. https://doi.org/10.19540/j.cnki.cjcmm.20211110.303.

Guo, Y., Zhang, Y., Hong, K., et al, 2014. AMPK inhibition blocks ROS-NFkappaB signaling and attenuates endotoxemia-induced liver injury. PLoS One. 9,. https://doi.org/10.1371/journal.pone.0086881 e86881.

Han, N.R., Moon, P.D., Ryu, K.J., et al, 2017. beta-eudesmol suppresses allergic reactions via inhibiting mast cell degranulation. Clin. Exp. Pharmacol. Physiol. 44, 257–265. https://doi.org/10.1111/1440-1681.12698.

Hayden, M.S., Ghosh, S., 2008. Shared principles in NF-kappaB signaling. Cell 132, 344–362. https://doi.org/10.1016/j.cell.2008.01.020.

Hazrati, S., Ebadi, M.T., Mollaei, S., et al, 2019. Evaluation of volatile and phenolic compounds, and antioxidant activity of different parts of *Ferulago angulata* (schlecht.). Boiss. Ind. Crop. Prod. 140. https://doi.org/10.1016/j.indcrop.2019.111589.

Hazrati, S., Govahi, M., Sedaghat, M., et al, 2020. A comparative study of essential oil profile, antibacterial and antioxidant activities of two cultivated *Ziziphora species (Z. clinopodioides and Z. tenuior)*. Ind. Crop. Prod. 157. https://doi.org/10.1016/j.indcrop.2020.112942.

Jiang, F.S., Li, M.Y., Wang, H.Y., et al, 2019. Coelonin, an anti-inflammation active component of *Bletilla striata* and its potential mechanism. Int. J. Mol. Sci. 20, 4422. https://doi.org/10.3390/ijms20184422.

Kim, H.Y., Nam, S.Y., Hwang, S.Y., et al, 2016. Atractylone, an active constituent of KMP6, attenuates allergic inflammation on

allergic rhinitis in vitro and in vivo models. Mol. Immunol. 78, 121–132. https://doi.org/10.1016/j.molimm.2016.09.007.

Kumar, J., Haldar, C., Verma, R., 2021. Melatonin ameliorates LPS-induced testicular nitro-oxidative stress (iNOS/TNFα) and inflammation (NF-kB/COX-2) via modulation of SIRT-1. Reprod. Sci. 28, 3417–3430. https://doi.org/10.1007/s43032-021-00597-0.

Liu, T.F., Xiao, B.W., Xiang, F., et al, 2020. Ultrasmall copper-based nanoparticles for reactive oxygen species scavenging and alleviation of inflammation related diseases. Nat. Commun. 11, 2788–2803. https://doi.org/10.1038/s41467-020-16544-7.

More, G.K., Makola, R.T., 2020. In-vitro analysis of free radical scavenging activities and suppression of LPS-induced ROS production in macrophage cells by *Solanum sisymbriifolium* extracts. Sci. Rep. 10, 6493. https://doi.org/10.1038/s41598-020-63491-w.

Nathan, C., 2002. Points of control in inflammation. Nature 420, 846–852. https://doi.org/10.1038/nature01320.

Nathan, C., Ding, A., 2010. Nonresolving inflammation. Cell 140, 871–882. https://doi.org/10.1016/j.cell.2010.02.029.

Neuder, L.E., Keener, J.M., Eckert, R.E., et al, 2009. Role of p38 MAPK in LPS induced pro-inflammatory cytokine and chemokine gene expression in equine leukocytes. Vet. Immunol. Immunopathol. 129, 192–199. https://doi.org/10.1016/j.vetimm.2008.11.006.

Nishanth, R.P., Jyotsna, R.G., Schlager, J.J., et al, 2011. Inflammatory responses of RAW 264.7 macrophages upon exposure to nanoparticles: role of ROS-NFkappaB signaling pathway. Nanotoxicology 5, 502–516. https://doi.org/10.3109/17435390.2010.541604.

Oh, B.M., Lee, S.J., Park, G.L., et al, 2019. Erastin inhibits septic shock and inflammatory gene expression via suppression of the NF-kappaB pathway. J. Clin. Med. 8, 2210–2222. https://doi.org/10.3390/jcm8122210.

Peng, W., Han, T., Xin, W.B., et al, 2010. Comparative research of chemical constituents and bioactivities between petroleum ether extracts of the aerial part and the rhizome of *Atractylodes macrocephala*. Med. Chem. Res. 20, 146–151. https://doi.org/10.1007/s00044-010-9311-8.

Reuter, S., Gupta, S.C., Chaturvedi, M.M., et al, 2010. Oxidative stress, inflammation, and cancer: how are they linked? Free. Radic. Biol. Med. 49, 1603–1616. https://doi.org/10.1016/j.freeradbiomed.2010.09.006.

Srećković, N., Katanić Stanković, J.S., Matić, S., et al, 2020. *Lythrum salicaria* L. (Lythraceae) as a promising source of phenolic compounds in the modulation of oxidative stress: comparison between aerial parts and root extracts. Ind. Crop. Prod. 155. https://doi.org/10.1016/j.indcrop.2020.112781.

Tu, W.J., Wang, H., Li, S., et al, 2019. The anti-inflammatory and anti-oxidant mechanisms of the Keap1/Nrf2/ARE signaling pathway in chronic diseases. Aging Dis. 10, 637–651. https://doi.org/10.14336/AD.2018.0513.

Wang, Y., Wang, G.Z., Rabinovitch, P.S., et al, 2014. Macrophage mitochondrial oxidative stress promotes atherosclerosis and nuclear factor-kappaB-mediated inflammation in macrophages. Circ. Res. 114, 421–433. https://doi.org/10.1161/CIRCRESAHA.114.302153.

Wu, Y.X., Lu, W.W., Geng, Y.C., et al, 2020. Antioxidant, antimicrobial and anti-inflammatory activities of essential oil derived from the wild rhizome of *Atractylodes macrocephala*. Chem. Biodivers. 17,. https://doi.org/10.1002/cbdv.202000268 e2000268.

Xiang, X.L., Cao, N., Chen, F.Y., et al, 2020. Polysaccharide of *Atractylodes macrocephala* Koidz (PAMK) alleviates cyclophosphamide-induced immunosuppression in mice by upregulating CD28/IP3R/PLCgamma-1/AP-1/NFAT signal pathway. Front. Pharmacol. 11,. https://doi.org/10.3389/fphar.2020.529657 529657.

Yao, Y., Liu, K. H., Zhao, Y., et al., 2018. Pterostilbene and 4'-Methoxyresveratrol Inhibited Lipopolysaccharide-Induced Inflammatory Response in RAW264.7 Macrophages. Molecules. 23, https://doi.org/10.3390/molecules23051148.

Yosr, Z., Imen, B.H.Y., Rym, J., et al, 2018. Sex-related differences in essential oil composition, phenol contents and antioxidant activity of aerial parts in *Pistacia lentiscus* L. during seasons. Ind. Crop. Prod. 121, 151–159. https://doi.org/10.1016/j.indcrop.2018.04.067.

Zamyatina, A., Heine, H., 2020. Lipopolysaccharide recognition in the crossroads of TLR4 and caspase-4/11 mediated inflammatory pathways. Front. Immunol. 11,. https://doi.org/10.3389/fimmu.2020.585146 585146.

Zhu, B., Zhang, Q.L., Hua, J.W., et al, 2018. The traditional uses, phytochemistry, and pharmacology of *Atractylodes macrocephala* Koidz.: a review. J. Ethnopharmacol. 226, 143–167. https://doi.org/10.1016/j.jep.2018.08.023.